Doménech Carbó, A.; Sabate-Fornons, F.; Sabater Picot, MJ. (24-0). Electrochemical Analysis of Catalytic and Oxygen Interfacial Transfer Effects on MnO2 Deposited on Gold Electrodes. The Journal of Physical Chemistry C. 122(20):10339-10947. https://doi.org/10.1021/acs.jpcc.8b02684

THE JOURNAL OF PHYSICAL CHEMISTRY C

Article

pubs.acs.org/JPCC

Electrochemical Analysis of Catalytic and Oxygen Interfacial Transfer Effects on MnO_2 Deposited on Gold Electrodes

Antonio Doménech-Carbó,*[,†] Ferran Sabaté,[‡] and Maria J. Sabater*[,‡]

[†]Departament de Química Analítica, Universitat de València, Dr. Moliner, 50, 46100 Burjassot, València, Spain

[‡]Instituto de Tecnología Química, Universitat Politècnica de València, Consejo Superior de Investigaciones Científicas, Av. Los Naranjos S/N, 46022 València, Spain

ABSTRACT: A theoretical model for obtaining thermochemical and kinetic information on oxygen interfacial transfer in metal oxides deposited on gold electrodes, based in the voltammetry of immobilized particle methodology, is presented. It is applied to MnO_2 microparticulate deposits on gold in contact with aqueous NaOH solution using the voltammetric signals for the oxidation of gold to gold oxide monolayer and its subsequent desorptive reduction. Assuming reversibility, voltammetric peak potentials permit to estimate a variation of Gibbs free energy of interfacial oxygen transfer of -32 ± 3 kJ mol^{-1}. Analysis of peak current data based on the Sharp−Hancock formalism of solid-state kinetics was consistent with the diffusive nature of the transfer process and permitted the separation between this effect and the catalytic effect exerted by MnO_2 on the electrochemical oxidation of gold.

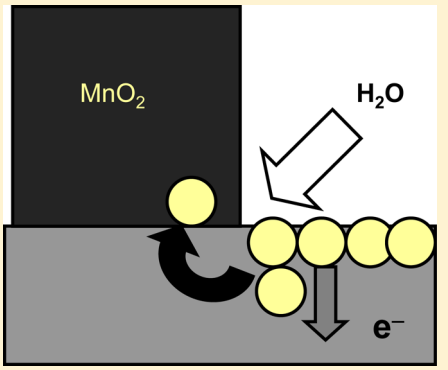

1. INTRODUCTION

The movement of chemical species adsorbed or formed on the outer surface of an oxide is a general phenomenon closely related to the ability of these materials to act on catalysis.[1] In particular, the observed spillover phenomenon in metal/oxide-based catalysts (i.e., Pt/TiO_2), which consists of the spreading of chemical species through the oxidic support after being activated by a metal, as well as the spreading toward the metal (back-spillover) has pushed the researchers to study this effect carefully under different perspectives,[2−4] in particular, the electrochemical promotion of catalytic reactions by means of solid electrolytes interfaced with noble metal electrodes studied by Vayenas, Toghan, and Imbihl et al.[5−7]

In this context, different research groups proved the existence of a phase change by oxygen on Pt/CeO_2 and Mn_2O_3−Na_2WO_4/SiO_2 by FT-Raman, electron spin resonance spectroscopy, electron paramagnetic resonance, and X-ray absorption near-edge structure.[8,9] Along with these techniques, electrochemical methodologies have also been applied to study the interfacial movement of chemical species on metal oxides (MOs). Among them, preliminary attempts to show the catalytic role of Pt/TiO_2 in the dynamic oxygen effusion by a potential dynamic sweep method must be highlighted.[10]

Following this work, Jaksic et al.[11−13] showed that water molecules underwent spontaneous dissociative adsorption on high-valent-modified MO electrodes (i.e., titania, tungsten, niobia, and tantalum oxides). Then, a sharp increase in the dissociation of water molecules was observed in the presence of metal nanoparticles (showing a catalytic role of the latter in the process) together with hydroxyl transference (OH^-) from one phase to another. In this case, potentiodynamic evidence for this event could be obtained.[14,15] In these cases, the electrochemical systems were based on MOs associated to Au and Pt electrodes: from plasma discharge-assisted metal-coating on pressed MO cylinders[16] to sol−gel MO deposition onto Pt electrodes[10−12] and impregnation of an MO deposit with H_2PtCl_6,[10] providing qualitative and semiquantitative monitoring of these processes.

With these precedents and in our aim to electrochemically identify oxygen-transfer effects on materials with a remarkable lattice oxygen release ability on cryptomelane-type MnO_2,[17−27] we have conducted a study of oxygen spillover effects using voltammetry of immobilized particle (VIMP) methodology on gold electrodes. This technique, developed by Scholz et al.,[28,29] provides analytical information on a variety of sparingly soluble solids upon attachment of micro or submicrosamples of the same to inert electrodes in contact with suitable electrolytes.[30]

Then, MnO_2-modified gold electrodes were prepared by drop-casting method on microcrystalline gold electrodes,[31,32] differing but in close analogy to classic impregnation methods for preparing metal-based catalysts.[11,33] Following the VIMP methodology, the MO forms a microparticulate deposit on the base gold electrode. As discussed below, this procedure avoids barrier effects associated to the more or less thick deposition of Pt and Au and provides a homogeneous distribution of the MO particles onto the electrode surface.[31,32]

These experiments will show that peak current ratios determined at different potential scan rates and switching potentials for the metal oxidation and their subsequent desorptive reduction can in principle be used to measure the

Received: March 20, 2018
Revised: April 24, 2018
Published: May 1, 2018

DOI: 10.1021/acs.jpcc.8b02684
J. Phys. Chem. C XXXX, XXX, XXX−XXX

extent of the interfacial oxygen-transfer effect from the gold electrode to the oxide (and vice versa) from simple voltammetric experiments. Theoretical modeling for electron-transfer processes on microparticulate deposits will be presented, following previous guidelines from VIMP,[34] to obtain thermodynamic and mechanistic information using, exclusively, an analysis of voltammetric parameters. Finally, on the bases of the electrochemical monitoring of MnO_2-modified gold electrodes and in the search for representative kinetics of this oxygen migration phenomenon, we have obtained linear graphs whose slope was consistent with a diffusion-controlled mechanism.

2. EXPERIMENTAL SECTION

Electrochemical experiments were performed at microparticulate deposits of MnO_2 deposited onto Au electrodes in contact with 1.0 M NaOH aqueous solutions, optionally deaerated by bubbling Ar for 10 min. Drop-casting conditioning of the working electrode was performed by evaporating 50 μL of a suspension of the solid material in ethanol (1 mg mL^{-1}) on the surface of the Au electrode. The electrode was previously polished with alumina slurry and rinsed with water and ethanol and sonicated in water for 10 min. Voltammetric measurements were performed in a conventional electrochemical cell using Au working electrodes (BAS MF 2012, geometrical area 0.018 cm^2), a Pt mesh auxiliary electrode, and a Pt wire pseudoreference electrode using a CH I660 potentiostat. The potentials are referred to Ag/AgCl via calibration of the Pt pseudoreference electrode in 1.0 mM $K_4Fe(CN)_6$ solution in 0.10 M KCl.

3. RESULTS AND DISCUSSION

3.1. Voltammetric Pattern. Figure 1 depicts the initial anodic scan cyclic voltammograms (three successive scans)

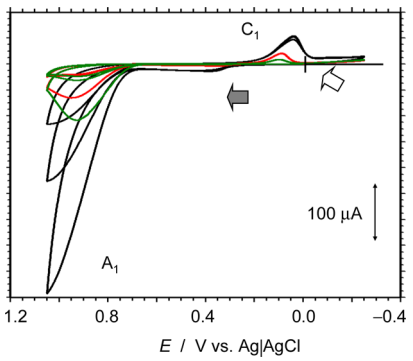

Figure 1. Cyclic voltammograms (three successive scans) of the Au electrode in 1.0 M NaOH. Potential scan initiated at 0.0 V (white arrow) in the positive direction (gray arrow); switching potential of 1.05 V; and sweep rate of 20 (red), 50 (green), and 200 (black) mV s^{-1}.

recorded at the Au electrode in 1.0 M NaOH at a switching potential of 1.05 V and varying potential scan rate (ν) between 20 and 200 mV s^{-1}. In the anodic scan, an oxidation wave ca. 1.0 V versus Ag/AgCl (A_1) was recorded followed, in the subsequent cathodic scan, by a tall reduction peak (C_1) at ca. +0.10 V. Under these experimental conditions, the oxygen evolution reaction (OER) appears as a rising current at the extreme of positive potentials ca. +1.5 V.

The process A_1, in agreement with abundant literature on Pt and Au electrochemistry,[35−44] can be described in terms of the formation of an adsorptive primary oxide layer and its subsequent cathodic desorption. For simplicity, the formation of the primary oxide monolayer can be represented as[42]

$$Au + 3H_2O \rightarrow Au(OH)_3 + 3H_{aq}^{+} + 3e^{-} \quad (1)$$

The cathodic process C_1 involves the reduction of oxidized gold species to gold metal. The large potential separation between the processes A_1 and C_1 has received different interpretations. By the one hand, the oxide monolayer can be dehydrated to form Au_2O_3[43]

$$Au(OH)_3 \rightarrow (1/2)Au_2O_3 + (3/2)H_2O \quad (2)$$

and can experience successive electrochemical reactions at more positive potentials[43]

$$Au(OH)_3 + Au + H_2O \rightarrow 2AuO(OH) + 3H^{+} + 3e^{-} \quad (3)$$

$$5AuO(OH) \rightarrow 2Au_2O_3 + Au + 2O_2 + 5H^{+} + 5e^{-} \quad (4)$$

The last process can be viewed as producing a catalytic effect on OER, already seen as involving intermediate hydroperoxy species.[42,43] As a result, the process C_1 would correspond to the reduction of Au_2O_3 to Au[41−43]

$$(1/2)Au_2O_3 + 3H_{aq}^{+} + 3e^{-} \rightarrow Au + (3/2)H_2O \quad (5)$$

Figure 2 compares the voltammetric response of an unmodified Au electrode with that of the same electrode modified with a microparticulate deposit of MnO_2 in contact with 1.0 M NaOH. On comparing such voltammograms, the more remarkable features are the increase of the intensity of the A_1 signal ($i_p(A_1)$) relative to the signal C_1 ($i_p(C_1)$) occurring on the MnO_2-modified electrode relative to the unmodified gold

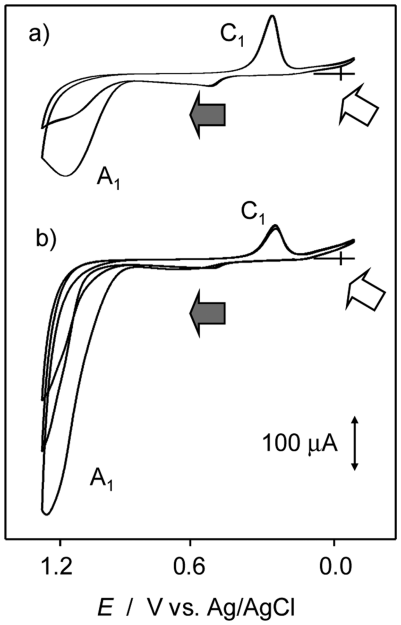

Figure 2. Cyclic voltammograms (two or three successive scans) of (a) unmodified Au and (b) MnO_2-modified Au electrodes immersed into 1.0 M NaOH. Potential scan initiated at 0.0 V (white arrow) in the positive direction (gray arrow); potential scan rate 50 mV s^{-1}; and switching potential 1.05 V.

DOI: 10.1021/acs.jpcc.8b02684
J. Phys. Chem. C XXXX, XXX, XXX−XXX

electrode and the slight variation in the position of the C_1 signal.

Another interesting contrast between modified and unmodified Au electrodes was observed on comparing the peak current for the anodic peak A_1 in first and second potential scans [$i_p(A_1)$ and $i_{p2}(A_1)$, respectively]. In the case of unmodified Au (Figures 1 and 2a), the $i_{p2}(A_1)/i_p(A_1)$ ratio is clearly lower than the corresponding ratio at MnO_2-modified electrodes (Figure 2b).

Another potentially interesting feature can be observed on comparing the significant differences in the $i_p(C_1)/i_p(A_1)$ ratio. Figure 3 depicts the variation of the above peak current ratio on

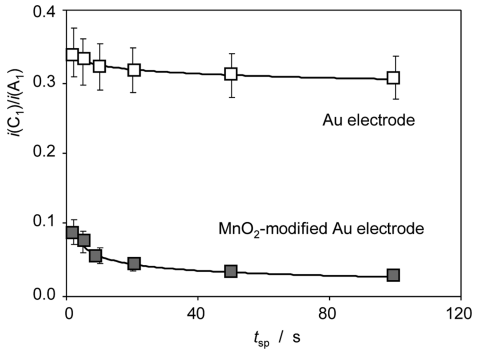

Figure 3. Variation of the $i_p(C_1)/i_p(A_1)$ ratio on the spillover time, t_{sp}, determined for unmodified and MnO_2-modified gold electrodes in contact with 1.0 M NaOH. Potential scan initiated at 0.0 V in the positive direction and switching potential 1.15 V.

the time associated to the spillover processes, t_{sp}, calculated as the ratio between the peak potential difference between peaks A_1 and C_1 and the potential scan rate v. Data for sweep rates between 10 and 500 mV s^{-1} provided a slow decrease of the ratio on the $i_p(C_1)/i_p(A_1)$ ratio with t_{sp}. As will be discussed in the following sections, these electrochemical parameters can in principle be used to measure the extent of the spillover effect from simple voltammetric experiments.

3.2. Catalytic and Interfacial Oxygen-Transfer Effects.

The observed voltammetric features can be rationalized on considering that the microparticulate deposit of the catalyst forms a discontinuous film of the Au electrode so that, as described in the models for the electrochemistry of ion-insertion solids: in both "direct" electrochemical[45−49] and electrocatalytic[50,51] processes, the electrochemical response is associated to the coupled charge transfer of electrons and charge-balancing electrolyte ions occurring at the particle/base electrode/electrolyte three-phase junction. Then, the voltammetric response of the catalyst-modified electrodes in the potential region where the A_1/C_1 processes occur is representative of the response of the uncovered fraction of Au electrode plus the response of the microparticulate system. Here, an interaction mechanism similar to that proposed for tungsten oxides can be hypothesized[12,52]

$$MnO_2 + xH_2O \rightarrow MnO_{2-x}(OH)_{2x} \quad (6)$$

$$MnO_{2-x}(OH)_{2x} + yAu \rightarrow yAu(OH)_3 + MnO_{2-x}(OH)_{2x-3y}^{3y+} + 3ye^- \quad (7)$$

$$MnO_{2-x}(OH)_{2x-3y}^{3y+} \rightarrow MnO_2 + (x-3y)H_2O + 3yH_{aq}^+ \quad (8)$$

occurring at the MnO_2 particle/gold electrode/electrolyte three-phase junction. Notice that the sum of the above processes yields the reaction described by eq 1. In this scheme, eq 7 can be viewed as an oxidative OH^- transfer yielding the gold oxide monolayer, subsequently experiencing competing processes described by eqs 3 and 4. Accordingly, the presence of MnO_2 determines a catalytic enhancement of the A_1 process of gold oxidation and OER, as observed on comparing Figure 2a,b.

Coupled to these processes, oxygen transfer and back-transfer effects can be represented, mimicking the scheme proposed by Lin,[11] in terms of oxygen migration within the MnO_2 lattice occupying interstitial positions (see schematics in

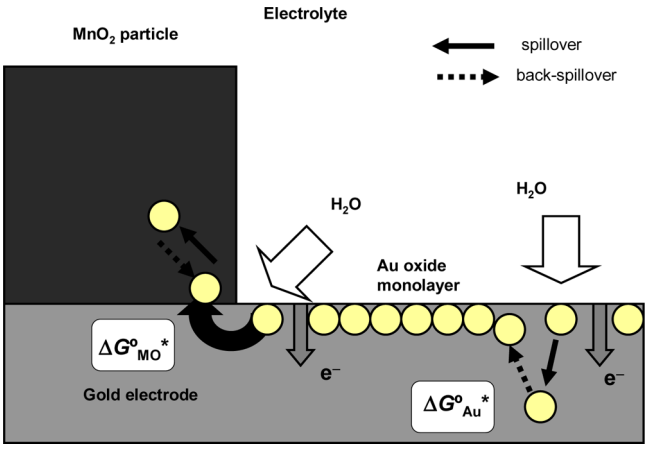

Figure 4. Simplified schematics for the electron-transfer and spillover (black arrows) and back-spillover processes occurring at MnO_2-modified Au electrodes in contact with an alkaline electrolyte.

Figure 4) occurring in parallel to the processes described by eqs 6−8.

$$2zAu(OH)_3 + MnO_{2-x}(OH)_{2x-3y}^{3y+} \rightarrow z\{Au_2O_3\}^* + \{MnO_{2-x}(OH)_{2x-3y+3z}^{(3y-z)+}\}^* + 3zH_{aq}^+ \quad (9)$$

followed by the MnO_2 formation analogue to eq 8

$$\{MnO_{2-x}(OH)_{2x-3y+3z}^{(3y-z)+}\}^*\{MnO_2\}^* + (x-3y+3z)H_2O + (3y-z)H_{aq}^+ \quad (10)$$

where the asterisk denotes the species after spillover transference of oxygens. Such processes provide a second way to form Au_2O_3 alternative to that described by eqs 1−4 occurring at unmodified gold electrodes.

3.3. Thermochemical calculations.

At the unmodified gold electrode, the Gibbs free energy in standard conditions associated to the anodic process described by eq 1, ΔG°_{A1}, can be calculated from the (apparent) equilibrium potential (E°_{A1}) using the Nernst equation as $\Delta G_{A1} = 3FE^\circ_{A1}$. In turn, the Gibbs free energy under identical conditions for the oxidation process

DOI: 10.1021/acs.jpcc.8b02684
J. Phys. Chem. C XXXX, XXX, XXX−XXX

C_1, ΔG_{C1}, described by eq 5, will be $\Delta G_{C1} = -3FE^\circ_{C1}$, E°_{C1} being the corresponding equilibrium potential.

In cyclic voltammetric experiments at relatively high potential scan rates (v) and/or at switching potentials (E_{lim}) close to the peak A_1, one can assume that there is no significant oxygen diffusion beyond the oxide monolayer. Then, assuming electrochemical reversibility, the potential separation between the processes A_1 and C_1 will permit to calculate the Gibbs free energy for the conversion of the gold oxide monolayer into gold oxide without spillover, described by eq 2, ΔG°_2, as

$$\Delta G^\circ_2 = -\Delta G^\circ_{A1} - \Delta G^\circ_{C1} = 3F(E^\circ_{C1} - E^\circ_{A1})_{v\to\infty} \quad (11)$$

Assuming that the potential range is confined to a region where the processes described by eqs 3 and 4 do not occur, in the voltammograms recorded at low scan rates and/or high switching potentials, spillover operates. This can be formally represented in terms of the conversion of Au_2O_3 into an O-intercalated form, $\{Au_2O_3^*\}$, formally represented as

$$Au(OH)_3 + (1/2)Au_2O_3 \rightarrow (1/2)\{Au_2O_3^*\} + \{Au(OH)_3^*\} \quad (12)$$

this process being a Gibbs energy change of $\Delta G^{\circ *}_2$. Then, the reduction of the $\{Au_2O_3^*\}$ form to Au metal under these conditions

$$(1/2)\{Au_2O_3^*\} + 3H^+ + 3e^- \rightarrow Au + (3/2)H_2O \quad (13)$$

will occur at a potential differing from that recorded at high scan rates, in which no oxygen transport occurs. Accordingly, as schematized in the thermochemical cycle depicted in Figure 5,

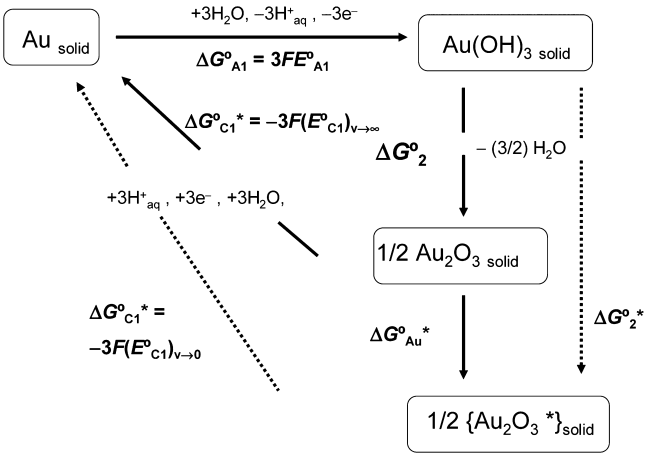

Figure 5. Thermochemical cycle corresponding to the oxygen transport associated to the electrochemical oxidation/reduction of Au electrodes in contact with aqueous alkaline media.

the difference $E_{C1} - E_{A1}$ should tend to a different limiting value $(E_{C1} - E_{A1})_{v\to 0}$ corresponding to a Gibbs free energy $\Delta G^{\circ *}_2$

$$\Delta G^{\circ *'}_2 = 3F(E^\circ_{C1} - E^\circ_{A1})_{v\to 0} \quad (14)$$

so that the free energy for oxygen transference (see scheme in Figure 4), $\Delta G^{\circ *}_{Au}$, can be calculated as the difference between $\Delta G^{\circ *'}_2$ and ΔG°_2.

At MnO_2-modified gold electrodes and high scan rates, one can assume that the peak A_1 reflects mainly the oxidative process yielding the gold oxide monolayer described by eqs 6–8, which in principle will be equivalent, under conditions of thermodynamic control, to that described by eq 2. At low scan rates, however, the processes represented by eqs 9 and 10 operate and Au_2O_3 will be formed. A simplified view can be obtained on assuming that, at high scan rates and/or low switching potentials, the process A_1 corresponds to the MnO_2-assisted oxidation of gold preceded by the process 6, as

$$Au + MnO(OH)_2 + 2H_2O \rightarrow Au(OH)_3 + MnO_2 + 3H^+ + 3e^- \quad (15)$$

which is followed by the formation of Au_2O_3, subsequently reduced through the process C_1 (eq 5), formally regenerating the hydrated MnO_2 form as schematized in Figure 6 with a

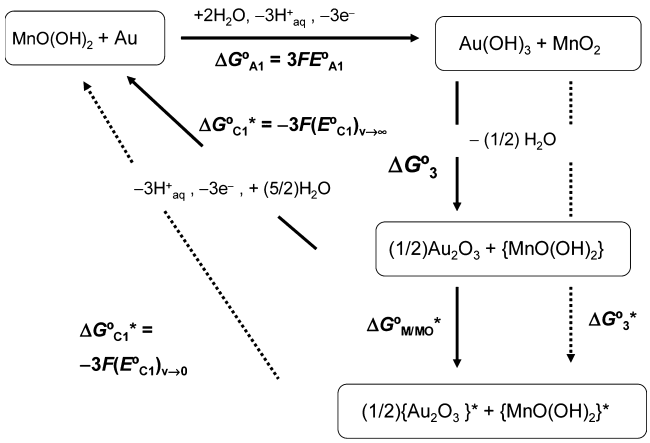

Figure 6. Thermochemical cycle for describing interfacial oxygen transport associated to the electrochemical oxidation/reduction of MnO_2-modified Au electrodes in contact with aqueous alkaline media.

change in the Gibbs free energy ΔG°_3. In the limiting case of low scan rates and/or high switching potentials, there will be reaction completion for processes 9 and 10 and there is interfacial O transport between the $Au(OH)_3$ monolayer and manganese oxide (see Figure 4). This process can be ideally represented as

$$Au(OH)_3 + MnO_2 \rightarrow (1/2)\{Au_2O_3^*\} + \{MnO(OH)_2^*\} + (1/2)H_2O \quad (16)$$

whose variation of the Gibbs free energy will be $\Delta G^{\circ *}_3$. Again, the subsequent electrochemical oxidation of the Au_2O_3 and $\{Au_2O_3^*\}$ forms to Au via the process C_1, formally regenerating MnO_2

$$(1/2)\{Au_2O_3\} + \{MnO(OH)_2\} + 3H^+ + 3e^- \rightarrow Au + MnO_2 + (5/2)H_2O \quad (17)$$

will differ at high scan rates, where there is no interfacial O transfer (and Au_2O_3 is formed), at high scan rates, where spillover occurs and $\{Au_2O_3^*\}$ is formed. Then, the difference between ΔG°_3 and $\Delta G^{\circ *}_3$ can be viewed as a measure of the variation of the Gibbs free energy associated to oxygen transfer/diffusion through the manganese oxide/gold oxide monolayer interface described by eq 16. Accordingly, the differences between the formal electrode potentials corresponding to the electrochemical processes C_1 and A_1 at low and high scan rates (and/or at very positive and slightly positive

DOI: 10.1021/acs.jpcc.8b02684
J. Phys. Chem. C XXXX, XXX, XXX−XXX

switching potentials) can be viewed as representative of the variation of the Gibbs energy associated to interfacial O transport, $\Delta G^{\circ}_{M/MO}$. This quantity can be calculated from the measured electrode potentials as

$$\Delta G^{\circ}_{M/MO} = \Delta G_3^{\circ *} - \Delta G_3^{\circ} = 3F[(E^{\circ}_{C1} - E^{\circ}_{A1})_{\nu\to 0} - (E^{\circ}_{C1} - E^{\circ}_{A1})_{\nu\to\infty}] \quad (18)$$

Figure 7a depicts the variation of the peak potential difference $(E_{C1} - E_{A1})$ on the switching potential for

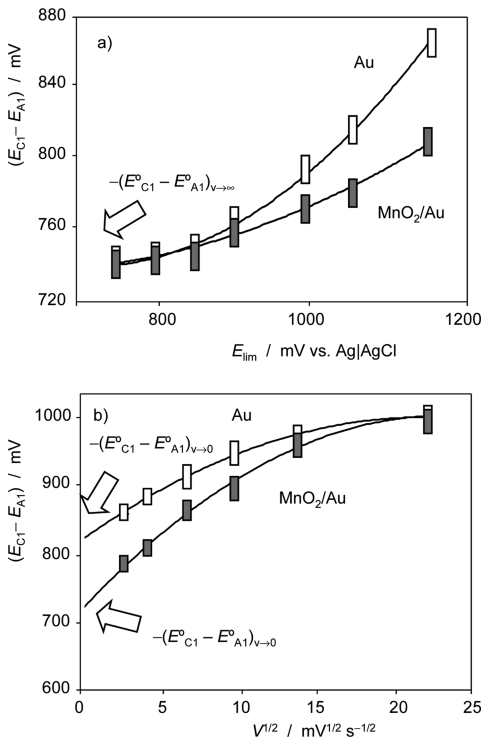

Figure 7. Variation of the peak potential difference $(E_{A1} - E_{C1})$ on: (a) the switching potential and (b) the potential scan rate for unmodified and MnO_2-modified gold electrodes in contact with 1.0 M NaOH. (a) Potential scan rate of 50 mV s^{-1} and (b) E_{lim} = 1.15 V vs Ag/AgCl.

unmodified and MnO_2-modified gold electrodes in contact with 1.0 M NaOH at the potential scan rate of 50 mV s^{-1}. Consistent with the foregoing set of considerations, at low E_{lim} values, the peak potential difference tends to a common limiting value for both electrodes [which can be taken as a measure of $(E^{\circ}_{C1} - E^{\circ}_{A1})_{\nu\to\infty}$], whereas at high E_{lim} values, the peak potential difference measured at Au and MnO_2–Au electrodes diverges.

For estimating $(E^{\circ}_{C1} - E^{\circ}_{A1})_{\nu\to 0}$, the values of the peak potential difference measured at a fixed E_{lim} (positive enough for producing a significant spillover effect) were plotted versus the potential scan rate, as described by Scholz et al. on studying tungsten bronze electrodes.[53] The corresponding representation can be seen in Figure 7b, where for smoothing the curved path of the graph, the square root of the scan rate was used as the x-axis. One can see in this figure that different values of $(E^{\circ}_{C1} - E^{\circ}_{A1})_{\nu\to 0}$ can be approximated at $\nu = 0$ for Au and MnO_2–Au electrodes. A small difference between $(E^{\circ}_{C1} - E^{\circ}_{A1})_{\nu\to 0}$ and $(E^{\circ}_{C1} - E^{\circ}_{A1})_{\nu\to\infty}$ determined for unmodified Au electrodes (10 ± 10 mV) can in principle be attributed to the appearance of the gold-localized spillover. This "internal spillover" can be associated to the diffusion of oxygen atoms within the gold matrix and would compete with the process described by eq 2. As expected, the difference between $(E^{\circ}_{C1} - E^{\circ}_{A1})_{\nu\to 0}$ and $(E^{\circ}_{C1} - E^{\circ}_{A1})_{\nu\to\infty}$ was clearly lower than that obtained for MnO_2–Au electrodes, 110 ± 10 mV, which permits to estimate $\Delta G^{\circ}_{M/MO}$ = −32 ± 3 kJ mol^{-1}. This value is clearly lower than those estimated for the activation energy for cation vacancy diffusion of Mn(II) in MnO (90–150 kJ mol^{-1})[54] and oxygen ion diffusion in $SrCe_{0.95}Yb_{0.05}O_3$ (92–109 kJ mol^{-1}),[55] but this discrepancy can in principle be explained by the occurrence of the oxygen-transfer process through the highly hydrated double-layer region formed at the metal–MnO_2 interface boundary, as schematized in Figure 8.

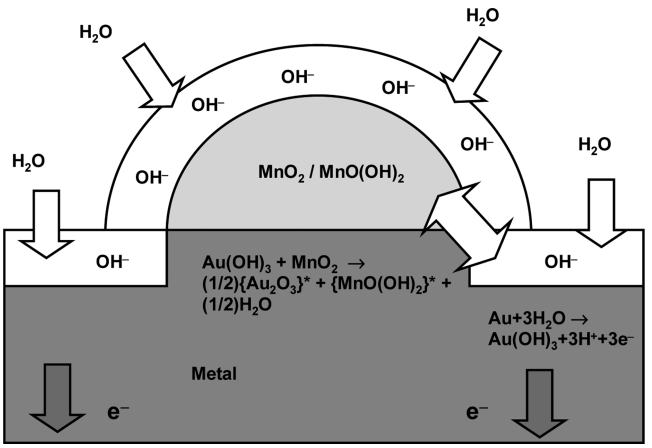

Figure 8. Schematics for the MnO_2-assisted electrochemical oxidation of gold in contact with an alkaline aqueous solution.

It is pertinent to note that this treatment is only a rough approximation by two main reasons: (i) the evaluation of thermochemical parameters requires strict electrochemical reversibility and (ii) the above treatment implies that the spillover process is not entirely reversed during the entire potential cycle. In spite of these limitations, the precedent treatment is able to compare the thermochemistry of spillover of different materials, of interest in the study of the catalytic performance of the same relative to selected chemical processes. Additionally, it is convenient to note that the systems studied here involve a solid–solid–liquid three-phase system differing from solid–solid–gas systems where spillover phenomena usually operate. Then, there is a variety of possibilities, for instance, processes involving low-concentration solution intermediates, requiring alternative formulations, in particular those leading to diffusion control.

3.4. Electrochemical Monitoring of Kinetic Aspects.

Let us consider the cyclic voltammetric response such as in Figures 1 and 2. The peak current for gold oxidation A_1 (eq 2) can be considered as proportional to the number of electrochemically accessible gold sites, n_o

$$i_a \approx \varepsilon_a n_o \quad (19)$$

ε_a being an electrochemical constant depending on the switching potential, scan rate, and so forth. In the subsequent cathodic scan, the peak current for the reduction of the gold oxide (eq 5) previously formed will be considered as proportional to the number of actives sites of gold oxide resulting from the sequence of processes described by eqs 3 and

DOI: 10.1021/acs.jpcc.8b02684
J. Phys. Chem. C XXXX, XXX, XXX–XXX

4. Assuming that during the electrochemical cycle some oxygen diffuses internally so that a certain fraction of gold oxidized in the process A_1 becomes inactive ("internal diffusion"), one can write

$$i_c \approx \varepsilon_c(n_o - n_{SAu}) \tag{20}$$

where ε_c is the corresponding electrochemical constant for the process C_1 and n_{SAu} denotes the number of gold sites deactivated as a result of internal oxygen diffusion. Assuming that this process advances with time during the voltammetric experiment, the i_c/i_a ratio for the bare gold electrode at a time t after generating the gold oxide monolayer will be

$$\left(\frac{i_c}{i_a}\right)_{Au}^{t} \approx \frac{\varepsilon_c(n_o - n_{SAu})}{\varepsilon_a n_o} = \left(\frac{\varepsilon_c}{\varepsilon_a}\right)\left(1 - \frac{n_{SAu}}{n_o}\right) \tag{21}$$

Accordingly, the fraction of gold sites undergoing internal diffusion at a time t can be approximated by

$$\left(\frac{n_{SAu}}{n_o}\right)_t = 1 - \left(\frac{\varepsilon_a}{\varepsilon_c}\right)\left(\frac{i_c}{i_a}\right)_{Au}^{t} \tag{22}$$

Extrapolating at time zero (i.e., in the limiting case of voltammetric experiments when no internal diffusion can occur), $n_{SAu} \to 0$, so that $i_c \approx \varepsilon_c n_o$ and then

$$\left(\frac{i_c}{i_a}\right)_{Au}^{t=0} = \left(\frac{\varepsilon_c}{\varepsilon_a}\right) \tag{23}$$

Accordingly, the n_{SAu}/n_o ratio can be calculated from peak current measurements as

$$\left(\frac{n_{SAu}}{n_o}\right)_t = 1 - \frac{\left(\frac{i_c}{i_a}\right)_{Au}^{t}}{\left(\frac{i_c}{i_a}\right)_{Au}^{t=0}} \tag{24}$$

Now, let us consider the cyclic voltammetric response at MnO_2-modified gold electrodes. Now, the current for gold oxidation is increased relative to that recorded at unmodified gold. Because, under our experimental conditions, MnO_2 forms a discontinuous particulate deposit onto the Au surface, the corresponding peak current can be written as the sum of that due to uncovered gold (eq 1) and that due to the catalytic effect exerted by MnO_2 (eq 7). Taking n_{MO} as the number of accessible gold sites for MnO_2-mediated oxidation of gold (representative of the electrocatalytic effect exerted by MnO_2 in this process), the peak current for the A_1 process will be

$$i_a \approx \varepsilon_a n_o + \varepsilon_{cat} n_{MO} \tag{25}$$

In the subsequent cathodic scan, the peak current for the reduction of the gold oxide previously formed will be considered as proportional to the number of actives sites of Au_2O_3 remaining after Au/MnO_2 interfacial transfer and internal oxygen diffusion on gold.

$$i_c \approx \varepsilon_c(n_o + n_{MO} - n_{SAu} - n_{SMO}) \tag{26}$$

n_{SMO} being the number of active gold sites which remain associated to oxygen diffused into MnO_2 (eqs 9 and 10). Then, the i_c/i_a ratio for the MnO_2-modified gold electrode at a time t after generating the gold oxide monolayer will be

$$\left(\frac{i_c}{i_a}\right)_{AuMO}^{t} \approx \frac{\varepsilon_c(n_o + n_{MO} - n_{SAu} - n_{SMO})}{\varepsilon_a n_o + \varepsilon_{cat} n_{MO}} = \left(\frac{\varepsilon_c}{\varepsilon_a}\right)\left(\frac{1 + n_{MO}/n_o - n_{SAu}/n_o - n_{SMO}/n_o}{1 + (\varepsilon_{cat}/\varepsilon_a)(n_{MO}/n_o)}\right) \tag{27}$$

Assuming, as before, that at time zero there is no spillover, the i_c/i_a ratio will be

$$\left(\frac{i_c}{i_a}\right)_{AuMO}^{t=0} \approx \frac{\varepsilon_c(n_o + n_{MO})}{\varepsilon_a n_o + \varepsilon_{cat} n_{MO}} = \left(\frac{\varepsilon_c}{\varepsilon_a}\right)\left(\frac{1 + n_{MO}/n_o}{1 + (\varepsilon_{cat}/\varepsilon_a)(n_{MO}/n_o)}\right) \tag{28}$$

As a result, eq 27 can be rewritten as

$$\left(\frac{i_c}{i_a}\right)_{AuMO}^{t} = \left(\frac{1 + n_{MO}/n_o - n_{SAu}/n_o - n_{SMO}/n_o}{1 + n_{MO}/n_o}\right)\left(\frac{i_c}{i_a}\right)_{AuMO}^{t=0} \tag{29}$$

Assuming that the amount of MnO_2 deposited onto the electrode surface is clearly lower than n_o, a condition that applies when a thin layer of MO was deposited onto the gold electrode surface, one can approximate $n_{MO}/n_o \ll 1$. Then

$$\left(\frac{i_c}{i_a}\right)_{AuMO}^{t} \approx [1 - n_{SAu}/n_o - n_{SMO}/n_o]\left(\frac{i_c}{i_a}\right)_{AuMO}^{t=0} \tag{30}$$

Combining the above equation with eq 24, one obtains

$$\left(\frac{i_c}{i_a}\right)_{AuMO}^{t} \approx \left[\frac{\left(\frac{i_c}{i_a}\right)_{Au}^{t}}{\left(\frac{i_c}{i_a}\right)_{Au}^{t=0}} - \frac{n_{SMO}}{n_o}\right]\left(\frac{i_c}{i_a}\right)_{AuMO}^{t=0} \tag{31}$$

Accordingly, the n_{SMO}/n_o ratio at any time t can be estimated as

$$\frac{n_{SMO}}{n_o} \approx \frac{\left(\frac{i_c}{i_a}\right)_{Au}^{t}}{\left(\frac{i_c}{i_a}\right)_{Au}^{t=0}} - \frac{\left(\frac{i_c}{i_a}\right)_{AuMO}^{t}}{\left(\frac{i_c}{i_a}\right)_{AuMO}^{t=0}} \tag{32}$$

It is also interesting to evaluate the electrocatalytic activity of MnO_2 on gold oxidation (eqs 6–8). For this purpose, rearranging the terms in eq 29 and assuming as before that the amount of MnO_2 deposited onto the electrode surface is clearly lower than n_o, the ratio n_{MO}/n_o can be determined as

$$\frac{n_{MO}}{n_o} = \frac{\left(\frac{\varepsilon_a}{\varepsilon_c}\right)\left(\frac{i_c}{i_a}\right)_{AuMO}^{t=0} - 1}{1 - \left(\frac{\varepsilon_{cat}}{\varepsilon_c}\right)\left(\frac{i_c}{i_a}\right)_{AuMO}^{t=0}} \tag{33}$$

In regard to the oxygen spillover process, the values of the n_{SMO}/n_o ratio given by eq 29 can be considered as representative of the kinetics of that process. This can in principle be treated in terms of solid-state reaction kinetics where the above ratio can be seen as equivalent to the

DOI: 10.1021/acs.jpcc.8b02684
J. Phys. Chem. C XXXX, XXX, XXX−XXX

conversion fraction, α ($0 < \alpha < 1$), defined as the molar fraction of the obtained product and assuming that at the end of the reaction the reactant is quantitatively converted into the product. From the above α values, the different kinetic models can be tested using the Sharp–Hancock formalism,[56] extensively used for studying solid-state reaction kinetics.[57,58] The kinetics of solid-state reactions is in general represented by the generalized kinetic equation $d\alpha/dt = -kf(\alpha)$, where α denotes the fraction of the solid reagent converted into product at a time t and k represents a rate constant having $(\text{time})^{-1}$ dimensions. The function $f(\alpha)$, representative of the different types of reaction mechanisms, adopts, in several cases, a mathematical form which can be represented as

$$\ln[-\ln(1-\alpha)] = m \ln k + m \ln t \quad (34)$$

where m is a numerical coefficient characterizing the reaction mechanism. Consistent with the proposed treatment, plots of $\ln[-\ln(1-\alpha)]$ versus $\ln t$ based on different series of voltammetric experiments, (i) varying the potential scan rate at fixed E_{lim} and (ii) varying E_{lim} at a fixed v, produced essentially identical Sharp–Hancock plots, as can be seen in Figure 9 for

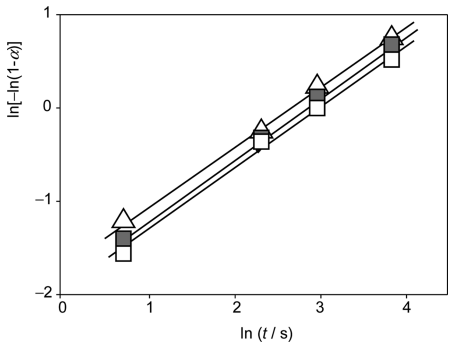

Figure 9. Sharp–Hancock representations of $\ln[-\ln(1-\alpha)]$ vs $\ln t$ for MnO_2-modified gold electrodes immersed into 1.0 M NaOH aqueous solution. From voltammetric data such as in Figure 2 varying v between 10 and 500 mV s^{-1} at E_{lim} = 1.15 V (squares), 1.05 V (solid squares), and 0.95 V (triangles).

experiments performed by varying v between 10 and 500 mV s^{-1} at E_{lim} = 1.15 V (squares), 1.05 V (solid squares), and 0.95 V (triangles). Remarkably, the slope of the Sharp–Hancock representations was in all cases around 0.60 ± 0.05, consistent with diffusion-controlled mechanisms,[56−58] providing averaged k values of $(4.5 \pm 1.2) \times 10^{-2}$.

4. CONCLUSIONS

Using the VIMP methodology, oxygen interfacial effects comparable to spillover processes on solid MnO_2-modified gold electrodes in contact with alkaline media can be monitored. Peak potential data for the gold oxidation process and its subsequent desorptive reduction can be used for approximating spillover thermochemical parameters, giving a variation of the Gibbs free energy for spillover of −32 ± 3 kJ mol^{-1}. Peak current ratios determined at different potential scan rates and different switching potentials for the above gold-localized voltammetric processes can be used to measure the extent of the spillover effect and separate the same from the electrocatalytic effect exerted by MnO_2 on gold oxidation. Kinetic analysis of voltammetric data for MnO_2-modified gold electrodes using the Sharp–Hancock formalism confirmed the diffusive nature of the spillover process and permitted to evaluate kinetic parameters for this process.

AUTHOR INFORMATION

Corresponding Authors

*E-mail: antonio.domenech@uv.es (A.D.-C.).
*E-mail: mjsabate@itq.upv.es (M.J.S.).

ORCID

Antonio Doménech-Carbó: 0000-0002-5284-2811

Notes

The authors declare no competing financial interest.

ACKNOWLEDGMENTS

Financial support by projects CTQ2014-53736-C3-2-P and CTQ2015-67592-P, which are supported with Ministerio de Economía, Industria y Competitividad (MINECO), and Fondo Europeo de Desarrollo Regional (ERDF) funds, and CTQ2017-85317-C2-1-P supported with funds from the MINECO, ERDF, and Agencia Estatal de Investigación (AEI) are gratefully acknowledged. F.S. acknowledges a PhD fellowship (Ayuda Predoctoral FPI Severo Ochoa) from MINECO.

REFERENCES

(1) Conner, W. C., Jr.; Falconer, J. L. Spillover in Heterogeneous Catalysis. *Chem. Rev.* **1995**, *95*, 759–788.
(2) Batley, G. E.; Ekstrom, A.; Johnson, D. A. Studies of topochemical heterogeneous catalysis: IV. Catalysis of the reaction of zinc sulphide with oxygen. *J. Catal.* **1975**, *36*, 285–290.
(3) Bond, G. C.; Molloy, L. R.; Fuller, M. J. Oxidation of carbon monoxide over palladium–tin(IV) oxide catalysts: an example of spillover catalysis. *J. Chem. Soc., Chem. Commun.* **1975**, 796–797.
(4) Chadwick, D.; Christie, A. B. Reactivity of lead monolayers on copper: evidence for oxygen spillover. *Vide, Couches Minces* **1980**, *201*, 423.
(5) Vayenas, C. G.; Bebelis, S.; Pliangos, C.; Brosda, S.; Tsiplakides, D. Electrochemical Activation of Catalysis: Promotion. In *Electrochemical Promotion, and Metal–Support Interactions*; Kluwer Academic/Plenum Publishers: New York, 2001.
(6) Toghan, A.; Rösken, L. M.; Imbihl, R. Origin of non-Faradayicity in electrochemical promotion of catalytic ethylene oxidation. *Phys. Chem. Chem. Phys.* **2010**, *12*, 9811–9815.
(7) Toghan, A.; Khodari, M.; Steinbach, F.; Imbihl, R. Microstructure of thin film platinum electrodes on yttrium stabilized zirconia prepared by sputter deposition. *Thin Solid Films* **2011**, *519*, 8139–8143.
(8) Li, C.; Song, Y.; Chen, Y.; Xin, Q.; Han, X.; Li, W. Spectroscopic studies of oxygen spillover on Pt/CeO_2 catalyst. *Stud. Surf. Sci. Catal.* **1997**, *112*, 439–446.
(9) Jiang, Z.-c.; Gong, H.; Li, S.-b. Methane activation over Mn_2O_3-Na_2WO_4/SiO_2 catalyst and oxygen spillover. *Stud. Surf. Sci. Catal.* **1997**, *112*, 481–490.
(10) Lin, H. The study of oxygen spillover and back spillover on Pt/TiO_2 by a potential dynamic sweep method. *J. Mol. Catal. A: Chem.* **1999**, *144*, 189–197.
(11) Jaksic, J. M.; Krstajic, N. V.; Vracar, L. M. Spillover of primary oxides as a dynamic catalytic effect of interactive hypo-d-oxide supports. *Electrochim. Acta* **2007**, *53*, 349–361.
(12) Jaksic, J. M.; Labou, D.; Papakonstantinou, G. D.; Siokou, A.; Jaksic, M. M. Novel Spillover Interrelating Reversible Electrocatalysts for Oxygen and Hydrogen Electrode Reactions. *J. Phys. Chem. C* **2010**, *114*, 18298–18312.
(13) Jaksic, J. M.; Labou, D.; Lacnjevac, C. M.; Siokou, A.; Jaksic, M. M. Potentiodynamic estimation of key parametric criterions and interrelating reversible spillover effects for electrochemical promotion. *Appl. Catal., A* **2010**, *380*, 1–14.

DOI: 10.1021/acs.jpcc.8b02684
J. Phys. Chem. C XXXX, XXX, XXX–XXX

(14) Neophytides, S. G.; Zafeiratos, S. H.; Jaksic, M. M. Selective Interactive Grafting of Composite Bifunctional Electrocatalysts for Simultaneous Anodic Hydrogen and CO Oxidation. *J. Electrochem. Soc.* **2003**, *150*, ES12−ES26.
(15) Livage, J.; Henry, M.; Sanchez, C. Sol-gel chemistry of transition metal oxides. *Prog. Solid State Chem.* **1988**, *18*, 259−341.
(16) Suh, M.; Bagus, P. S.; Pak, S.; Rosynek, M. P.; Lunsford, J. H. Reactions of Hydroxyl Radicals on Titania, Silica, Alumina, and Gold Surfaces. *J. Phys. Chem. B* **2000**, *104*, 2736−2742.
(17) Nicolas-Tolentino, E.; Tian, Z.-R.; Zhou, H.; Xia, G.; Suib, S. L. Effects of Cu^{2+} ions on the structure and reactivity of todorokite—and cryptomelane—type manganese oxide octahedral molecular sieves. *Chem. Mater.* **1999**, *11*, 1733−1741.
(18) Brock, S. L.; Duan, N.; Tian, Z. R.; Giraldo, O.; Zhou, H.; Suib, S. L. A review of porous manganese oxide materials. *Chem. Mater.* **1998**, *10*, 2619−2628.
(19) Ching, S.; Krukowska, K. S.; Suib, S. L. A new synthetic route to todorokite—type manganese oxides. *Inorg. Chim. Acta* **1999**, *294*, 123−132.
(20) Son, Y.-C.; Makwana, V. D.; Howell, A. R.; Suib, S. L. Efficient, catalytic, aerobic oxidation of alcohols with octahedral molecular sieves. *Angew. Chem., Int. Ed.* **2001**, *40*, 4280−4283.
(21) Sabaté, F.; Navas, J.; Sabater, M. J.; Corma, A. Synthesis of γ-lactones from easily and accessible reactants catalyzed by Cu−MnO_x catalysts. *C. R. Chim.* **2018**, *21*, 164−173.
(22) Corma, A.; Navas, J.; Ródenas, T.; Sabater, M. J. One-pot palladium-catalyzed borrowing hydrogen synthesis of thioethers. *Chem.—Eur. J.* **2013**, *19*, 17464−17471.
(23) Corma, A.; Navas, J.; Sabater, M. J. Coupling of two multistep catalytic cycles for the one-pot synthesis of propargylamines from alcohols and primary amines on a nanoparticulated gold catalyst. *Chem.—Eur. J.* **2012**, *18*, 14150−14156.
(24) Corma, A.; Ródenas, T.; Sabater, M. J. Aerobic oxidation of thiols to disulfides by heterogeneous gold catalysts. *Chem. Sci.* **2012**, *3*, 398−404.
(25) Corma, A.; Boronat, M.; Climent, M. J.; Iborra, S.; Montón, R.; Sabater, M. J. A recycable bifunctional acid−base organocatalyst with ionic liquid character. The role of site separation and spatial configuration on different condensation reactions. *Phys. Chem. Chem. Phys.* **2011**, *13*, 17255−17261.
(26) Climent, M. J.; Iborra, S.; Sabater, M. J.; Vidal, J. D. Bifunctional acid−base ionic liquid for the one-pot synthesis of fine chemicals: Thioethers, 2H-chromenes and 2H-quinoline derivatives. *Appl. Catal., A* **2014**, *481*, 27−38.
(27) Corma, A.; Navas, J.; Sabater, M. J. Advances in one-pot synthesis through borrowing hydrogen catalysis. *Chem. Rev.* **2018**, *118*, 1410−1459.
(28) Scholz, F.; Meyer, B. Voltammetry of Solid Microparticles Immobilized on Electrode Surfaces. In *Electroanalytical Chemistry, A Series of Advances*; Bard, A. J., Rubinstein, I., Eds.; Marcel Dekker: New York, 1998; Vol. *20*, pp 1−86.
(29) Scholz, F.; Schröder, U.; Gulaboski, R.; Doménech-Carbó, A. *Electrochemistry of Immobilized Particles and Droplets*, 2nd ed.; Springer: Berlin-Heidelberg, 2014.
(30) Doménech-Carbó, A.; Labuda, J.; Scholz, F. Electroanalytical chemistry for the analysis of solids: characterization and classification (IUPAC Technical Report). *Pure Appl. Chem.* **2013**, *85*, 609−631.
(31) Doménech-Carbó, A.; Koshevoy, I. O.; Montoya, N.; Pakkanen, T. A.; Doménech-Carbó, M. T. Solvent-Independent Electrode Potentials of Solids Undergoing Insertion Electrochemical Reactions: Part II. Experimental Data for Alkynyl-diphosphine Dinuclear Au(I) Complexes Undergoing Electron Exchange Coupled to Anion Exchange. *J. Phys. Chem. C* **2012**, *116*, 25984−25992.
(32) Doménech-Carbó, A.; Scholz, F.; Montoya, N. Solvent-Independent Electrode Potentials of Solids Undergoing Insertion Electrochemical Reactions: Part III. Experimental Data for Prussian Blue Undergoing Electron Exchange Coupled to Cation Exchange. *J. Phys. Chem. C* **2012**, *116*, 25993−25999.
(33) Mehrabadi, B. A. T.; Eskandari, S.; Khan, U.; White, R. D.; Regalbuto, J. R. A Review of Preparation Methods for Supported Metal Catalysts. *Adv. Catal.* **2017**, *61*, 1−35.
(34) Doménech-Carbó, A. Solvent-Independent Electrode Potentials of Solids Undergoing Insertion Electrochemical Reactions: Part I Theory. *J. Phys. Chem. C* **2012**, *116*, 25977−25983.
(35) Angerstein-Kozlowska, H.; Conway, B. E.; Hamelin, A.; Stoicoviciu, L. Elementary steps of electrochemical oxidation of single-crystal planes of Au—I. Chemical basis of processes involving geometry of anions and the electrode surfaces. *Electrochim. Acta* **1986**, *31*, 1051−1061.
(36) Angerstein-Kozlowska, H.; Conway, B. E.; Hamelin, A.; Stoicoviciu, L. Elementary steps of electrochemical oxidation of single-crystal planes of Au Part II. A chemical and structural basis of oxidation of the (111) plane. *J. Electroanal. Chem.* **1987**, *228*, 429−453.
(37) Conway, B. E.; Barnett, B.; Angerstein-Kozlowska, H.; Tilak, B. V. A surface-electrochemical basis for the direct logarithmic growth law for initial stages of extension of anodic oxide films formed at noble metals. *J. Chem. Phys.* **1990**, *93*, 8361−8373.
(38) Conway, B. E. Electrochemical oxide film formation at noble metals as a surface-chemical process. *Prog. Surf. Sci.* **1995**, *49*, 331−452.
(39) Chen, A.; Lipkowski, J. Electrochemical and Spectroscopic Studies of Hydroxide Adsorption at the Au(111) Electrode. *J. Phys. Chem. B* **1999**, *103*, 682−691.
(40) Burke, L. D.; O'Mullane, A. P. Generation of active surface states of gold and the role of such states in electrocatalysis. *J. Solid State Electrochem.* **2000**, *4*, 285−297.
(41) Burke, D. L.; O'Mullane, A. P.; Lodge, V. E.; Mooney, M. B. Auto-inhibition of hydrogen gas evolution on gold in aqueous acid solution. *J. Solid State Electrochem.* **2001**, *5*, 319−327.
(42) Doyle, R. L.; Lyons, M. E. G. The mechanism of oxygen evolution at superactivated gold electrodes in aqueous alkaline solution. *J. Solid State Electrochem.* **2014**, *18*, 3271−3286.
(43) Diaz-Morales, O.; Calle-Vallejo, F.; de Munck, C.; Koper, M. T. M. Electrochemical water splitting by gold: evidence for an oxide decomposition mechanism. *Chem. Sci.* **2013**, *4*, 2334−2343.
(44) Yeo, B. S.; Klaus, S. L.; Ross, P. N.; Mathies, R. A.; Bell, A. T. Identification of Hydroperoxy Species as Reaction Intermediates in the Electrochemical Evolution of Oxygen on Gold. *ChemPhysChem* **2010**, *11*, 1854−1857.
(45) Lovrić, M.; Scholz, F. A model for the propagation of a redox reaction through microcrystals. *J. Solid State Electrochem.* **1997**, *1*, 108−113.
(46) Oldham, K. B. Voltammetry at a three-phase junction. *J. Solid State Electrochem.* **1998**, *2*, 367−377.
(47) Lovrić, M.; Scholz, F. A model for the coupled transport of ions and electrons in redox conductive microcrystals. *J. Solid State Electrochem.* **1999**, *3*, 172−175.
(48) Schröder, U.; Oldham, K. B.; Myland, J. C.; Mahon, P. J.; Scholz, F. Modelling of solid state voltammetry of immobilized microcrystals assuming an initiation of the electrochemical reaction at a three-phase junction. *J. Solid State Electrochem.* **2000**, *4*, 314−324.
(49) Doménech, A. A model for solid-state voltammetry of zeolite-associated species. *J. Phys. Chem. B* **2004**, *108*, 20471−20478.
(50) Doménech, A.; Aucejo, R.; Alarcón, J.; Navarro, P. Electrocatalysis of the oxidation of methylenedioxyamphetamines at electrodes modified by cerium-doped zirconias. *Electrochem. Commun.* **2004**, *6*, 719−723.
(51) Doménech, A.; García, H.; Casades, I.; Esplá, M. Electrochemistry of 6-nitro-1′,3′,3′-trimethylspiro[2H-1-benzopyran-2,2′-indoline] Associated to Zeolite Y and MCM-41 Aluminosilicate. Site-Selective Electrocatalytic Effect on N, N,N′,N′-Tetramehtylbenzidine Oxidation. *J. Phys. Chem. B* **2004**, *108*, 20064−20075.
(52) Neophytides, S. G.; Murase, K.; Zafeiratos, S.; Papakonstantinou, G.; Paloukis, F. E.; Krstajic, N. V.; Jaksic, M. M. Composite hypo-hyper-d-intermetallic and interionic phases as supported interactive electrocatalysts. *J. Phys. Chem. B* **2006**, *110*, 3030−3042.

DOI: 10.1021/acs.jpcc.8b02684
J. Phys. Chem. C XXXX, XXX, XXX−XXX

(53) Cisternas, R.; Kahlert, H.; Wulff, H.; Scholz, F. The electrode responses of a tungsten bronze electrode differ in potentiometry and voltammetry and give access to the individual contributions of electron and proton transfer. *Electrochem. Commun.* **2015**, *56*, 34−37.
(54) De Souza, R. A.; Kilner, J. A.; Steele, B. C. H. A SIMS study of hydrogen in acceptor-doped perovskite oxides. *Solid State Ionics* **1995**, *77*, 180−184.
(55) Bertolo, E.; Kilner, J. A.; Sahibzada, M. Oxygen diffusion in $SrCe_{0.95}Yb_{0.05}O_{3-\delta}$. *J. Solid State Electrochem.* **2004**, *8*, 585−591.
(56) Hancock, J. D.; Sharp, J. H. Method of Comparing Solid-State Kinetic Data and Its Application to the Decomposition of Kaolinite, Brucite, and $BaCO_3$. *J. Am. Ceram. Soc.* **1972**, *55*, 74−77.
(57) Galwey, A. K.; Brown, M. E. Isothermical kinetic analysis of solid-state reactions using plots of rate against derivative function of the rate equation. *Thermochim. Acta* **1995**, *269−270*, 1−25.
(58) Mamleev, V.; Bourbigot, S.; Le Bras, M.; Duquesne, S.; Šesták, J. Modelling of nonisothermal kinetics in thermogravimetry. *Phys. Chem. Chem. Phys.* **2000**, *2*, 4708−4716.

DOI: 10.1021/acs.jpcc.8b02684
J. Phys. Chem. C XXXX, XXX, XXX−XXX